Elevated pCO_2 Impedes Succession of Phytoplankton Community From Diatoms to Dinoflagellates Along With Increased Abundance of Viruses and Bacteria

Ruiping Huang[1], Jiazhen Sun[2], Yunlan Yang[1], Xiaowen Jiang[2], Zhen Wang[3], Xue Song[2], Tifeng Wang[2], Di Zhang[2], He Li[2], Xiangqi Yi[1], Shouchang Chen[2], Nanou Bao[2], Liming Qu[2], Rui Zhang[3], Nianzhi Jiao[2], Yahui Gao[3], Bangqin Huang[1], Xin Lin[2], Guang Gao[2] and Kunshan Gao[2]*

[1] State Key Laboratory of Marine Environmental Science, College of the Environment and Ecology, Xiamen University, Xiamen, China, [2] State Key Laboratory of Marine Environmental Science, College of Ocean and Earth Sciences, Xiamen University, Xiamen, China, [3] School of Life Sciences, Xiamen University, Xiamen, China

Eutrophic coastal regions are highly productive and greatly influenced by human activities. Primary production supporting the coastal ecosystems is supposed to be affected by progressive ocean acidification driven by increasing CO_2 emissions. In order to investigate the effects of high pCO_2 (HC) on eutrophic plankton community structure and ecological functions, we employed 9 mesocosms and carried out an experiment under ambient ($\sim$410 ppmv) and future high (1000 ppmv) atmospheric pCO_2 conditions, using *in situ* plankton community in Wuyuan Bay, East China Sea. Our results showed that HC along with natural seawater temperature rise significantly boosted biomass of diatoms with decreased abundance of dinoflagellates in the late stage of the experiment, demonstrating that HC repressed the succession from diatoms to dinoflagellates, a phenomenon observed during algal blooms in the East China Sea. HC did not significantly influence the primary production or biogenic silica contents of the phytoplankton assemblages. However, the HC treatments increased the abundance of viruses and heterotrophic bacteria, reflecting a refueling of nutrients for phytoplankton growth from virus-mediated cell lysis and bacterial degradation of organic matters. Conclusively, our results suggest that increasing CO_2 concentrations can modulate plankton structure including the succession of phytoplankton community and the abundance of viruses and bacteria in eutrophic coastal waters, which may lead to altered biogeochemical cycles of carbon and nutrients.

Keywords: biogenic silica, community structure, eutrophic coasts, ocean acidification, plankton, viruses

INTRODUCTION

The ocean CO_2 sink has increased from 1.7 ± 0.4 Pg C yr^{-1} in 1980s to 2.5 ± 0.6 Pg C yr^{-1} in 2010s (Friedlingstein et al., 2020), leading to the pH drop of open ocean surface by 0.017–0.027 units per decade (IPCC, 2019), an environmental problem known as ocean acidification (OA). It is predicted that further reduction of around 0.3 pH units will occur by the end of this century under

"business as usual" scenario (IPCC, 2019). Considering the huge changes, it is needed to investigate how marine life will respond directly or indirectly and the consequent changes in biogeochemical cycles. A number of studies have been conducted ranging from single organism to artificial community then to natural community levels, using laboratory, mesocosm and field investigation approaches (see the review by Gao et al., 2019 and literatures therein).

Field mesocosm experiments using natural communities are becoming effective approaches to explore the responses of marine planktonic ecosystems to climate change. Two mesocosm studies deployed in the Raunefjorden, western Norway, showed that *Emiliania huxleyi*, the most abundant coccolithophore species, reduced its growth rates under 710 µatm of pCO$_2$ during May–June 2001 (Engel et al., 2005), and even lost blooming capacity under 1000–3000 µatm conditions during May–June 2011 (Riebesell et al., 2016). In another mesocosm experiment carried out in the Raunefjorden during May 2006, the dominant group of prasinophyte community changed from *Bathycoccus*-like phylotypes to *Micromonas*-like phylotypes, as pCO$_2$ increased from current to predicted future levels (Meakin and Wyman, 2011). These results suggest that the OA effects on community structure can vary temporally in the same regions. In addition, highly variable effects of elevated pCO$_2$ on plankton also attribute to different regions. Under HC conditions, the composition of the community from the temperate Bering Sea shelf and offshore shifted away from diatoms toward nanophytoplankton (Hare et al., 2007). In the temperate Gullmar Fjord at the Swedish west coast, the total diatom biomass were unaffected by pCO$_2$ during bloom processes, but displayed a positive response to pCO$_2$ during post-bloom processes (Bach et al., 2016). Off the subtropical eastern coast of Gran Canaria, Spain, the total diatom biomass remained unaffected during oligotrophic conditions, but was significantly positively affected by high CO$_2$ after nutrient enrichment (Bach et al., 2019). Other plankton also showed varied responses to OA among different regions. The development of zooplankton community was unaffected significantly in the temperate Kongsfjorden Fjord of northwestern Norway (Aberle et al., 2013; Niehoff et al., 2013), but was prevented by increased pCO$_2$ off the subtropical eastern coast of Gran Canaria, Spain (Riebesell et al., 2018). In the mesocosm experiment conducted in the Kongsfjorden Fjord, bacterioplankton diversity differed significantly between high and low pCO$_2$ treatments (Zhang et al., 2013). However, pCO$_2$ did not affect bacterioplankton diversity, in our previous mesocosm experiment conducted in the subtropical eutrophic Wuyuan Bay (Lin et al., 2018). The shifts in plankton community structure will further influence the ecological functions, such as the production, consumption and export of organic matter, with different magnitudes and even directions (de Kluijver et al., 2013; Spilling et al., 2016; Taucher et al., 2020). By integrating and analyzing the results of mesocosm experiments, we noted that planktonic ecosystem level responses to elevated pCO$_2$ can vary spatiotemporally, which may depend on the initial community structure and other abiotic environmental factors such as nutrient levels.

To date, most mesocosm experiments have been conducted in oligotrophic or non-eutrophicated regions. In the mesocosm experiment employed in the Kongsfjorden during June–July 2010, increase in pCO$_2$ did not significantly influence chlorophyll a (Chl a) concentration under oligotrophic conditions, but increased Chl a concentration after nutrient fertilization (Schulz et al., 2013). Increased pCO$_2$ similarly affected Chl a concentration after nutrient addition, in the mesocosm experiment employed in Raunefjord during May–June 2011 (Riebesell et al., 2016). In our previous mesocosm experiments which have been carried out in the highly eutrophic Wuyuan Bay, we found that HC treatment did not significantly affect Chl a concentration (Liu et al., 2017). The plankton community composition responses to increased pCO$_2$ also varied in different phases of the mesocosm experiment conducted in the Gullmar Fjord, resulting from plankton communities supported by regenerated nutrients were more sensitive to OA than those having access to higher availability of inorganic nutrients (Bach et al., 2017; Bach et al., 2019). These results suggested that planktonic ecosystem level responses to elevated pCO$_2$ can be influenced by nutrient levels.

Coastal waters are highly productive that support marine ecosystem and human activities. In these regions, the accumulative effects of natural and anthropogenic climate change are continuing and intensifying the course of eutrophication (Rabalais et al., 2009). With progressive OA, eutrophication is supposed to enhance the CO$_2$-driven acidification in coastal waters, by an additional drop of 0.13 pH unit relative to open oceans at the end of this century (Cai et al., 2011). Such enhanced OA in pH fluctuating coastal waters can disrupt ecosystem service due to increased energetic demand for ecosystems to sustain. To better understand the consequences of OA in eutrophic coastal regions, further studies should be expanded to look into the ecological responses in different regions and at different seasons under fluctuating and changing environmental conditions. Here, we carried out a mesocosm experiment in the eutrophic coastal region Wuyuan Bay, using *in situ* community during April–May 2018. Apart from monitoring environmental and biogenic changes, we particularly focused on the phytoplankton community succession and the abundance of viruses and bacteria, and the results showed notable correlation between autotrophic assimilation and heterotrophic dissimilation.

MATERIALS AND METHODS

Mesocosms Setup

The mesocosm experiment was conducted in the Facility for the Study of Ocean Acidification Impacts of Xiamen University, located in the subtropical coastal region Wuyuan Bay (24°31′48″ N, 118°10′47″ E), during 9th April–15th May 2018. Nine cylindrical mesocosm bags with 3 m in depth and 1.5 m in diameter, made of transparent thermoplastic polyurethane (TPU), were fixed within steel frames and sheltered by cone lids. The *in situ* seawater were filtered (pore size of 0.01 µm) by water purifier (MU801-4T, Midea, China) and pumped simultaneously into 9 mesocosm bags for 3000 L within 36 h. Bag 2, 4, 6, and

8 were set as control, aerated with ambient air pCO_2 (denoted as AC). To adjust seawater to projected 1000 µatm CO_2 in 2100, bag 1, 3, 5, 7, and 9 were added with approximately 11 L CO_2 saturation seawater (denoted as HC) (Riebesell et al., 2013). Subsequently, AC and HC mesocosm bags were aerated (5 L min^{-1}) with ambient air of ∼410 ppmv CO_2 and pre-mixed air-CO_2 of 1000 ppmv CO_2, respectively, till the end of the experiment. After aerating to homogenize the carbonate system for about 2–3 h, 720 L of *in situ* seawater filtered by 180 µm mash was added simultaneously into 9 mesocosm bags, so that each bag was inoculated with 80 L *in situ* seawater containing a natural microbe community. Subsequently, the mesocosm samples were collected from 0.5 m depths of each bag at 10:00 a.m. every 1–3 days, for physical, chemical and biological analysis.

Physical and Chemical Parameters Measurements

The intensity of solar irradiance was measured with a real-time solar irradiance monitoring device (EKO, Japan). Salinity and temperature were measured using a salinometer and digital thermometer, respectively. The pH was determined instantly using a pH meter (Orion Star A211, Thermo Scientific), which was calibrated against NIST-traceable pH buffers. Samples for dissolved inorganic carbon (DIC) measurements were poisoned with final concentration of 1‰ saturated $HgCl_2$ solution and stored in 40 mL borosilicate glass vials until further analysis. The DIC was determined by acidifying 0.5 mL samples and then measuring CO_2 concentration using a DIC analyzer (AS-C3, Apollo, United States). The other parameters of carbonate system were calculated from DIC and pH_{NBS} using CO2SYS program (Lewis and Wallace, 1998) based on known levels of nutrients, temperature, and salinity.

Samples for nutrient measurements were filtered through 0.45 mm cellulose acetate membrane by suction filter. The filtrate was divided into 2 of 125 mL high density polyethylene bottles: one was stored at $-20°C$ and measured concentrations of NO_3^-, NO_2^-, PO_4^{3-}, and SiO_3^{2-} using an auto-analyzer (AA3, Seal, Germany) at room temperature, and another added with 1‰ chloroform was stored at 4°C and measured concentration of NH_4^+ with indophenol blue spectrophotometry (Tri-223, Spectrum, China) at 25°C.

Chlorophyll *a* Measurement

Water samples of 250–1000 mL were filtered onto GF/F membranes by suction filter with low vacuum pressure (<0.02 MPa), and soaked in pure methanol at 40°C for 1 h. Then the extracts were centrifuged at 6000 × g for 10 min, and the absorption spectra of supernatants from 400 to 800 nm were measured using a UV-VIS Spectrophotometer (DU800, Beckman, United States). The Chl a concentration was calculated according to the equations from Ritchie (2006).

Viruses and Bacteria Abundance Measurement

Samples filtered by 20 µm mash were collected into 2 mL centrifuge tubes and fixed with glutaraldehyde to a final concentration of 0.5% at room temperature for 15 min, then frozen with liquid nitrogen and stored at $-80°C$ for further measurement. Viruses and bacteria were counted according to forward scatter, side scatter, and fluorescence intensity after samples were stained with SYBR Green I (Molecular Probe, United States), using the Epics Altra II flow cytometer (Beckman Coulter, United States) and Accuri C6 flow cytometer (Becton and Dickinson, United States), respectively (Chen et al., 2019). For the abundance measurement of both viruses and bacteria, fluorescent beads (Molecular Probes) with a diameter of 1 µm were added as an internal standard.

Phytoplankton Community Structure Determination

Water samples of 500–2000 mL were collected into polyethylene bottles and fixed by adding with 1% lugol's iodine. Then the samples were static placed, and concentrated to 25 mL using siphons within 3 days. The concentrated samples were observed using microscopy and plankton chamber to analyze phytoplankton abundance and diversity based on morphological characteristics.

Measurements of Primary Productivity and Respiratory Carbon Loss

Water samples of 120 mL were collected and transferred immediately into 6 glass scintillation vials (3 vials were used for 12 h inoculation and 3 vials were used for 24 h inoculation) before sunrise. The samples were inoculated with 100 µL of 5 µCi (0.185 MBq) $NaH^{14}CO_3$ solution (ICN Radiochemicals, United States) for 12 h and 24 h with similar levels of sunlight and temperature as in the mesocosms. After 12 and 24 h incubation, the cells were filtered onto glass-fiber filters (25 mm, Whatman GF/F, United States), and the filters were stored at $-20°C$. Later on, the filters were thawed and exposed to HCl fumes overnight and dried at 60°C for 6 h to remove unincorporated labeled carbon, then 3 ml of scintillation cocktail (Hisafe 3, Perkin-Elmer) was added. The incorporated radioactivity was measured by liquid scintillation counting (LS 6500, Beckman Coulter, United States). The respiratory carbon loss during night was calculated as the difference between carbon fixation of 12 h (day-time primary productivity) and 24 h (daily net primary productivity).

Biogenic Silica Measurement

Water samples of 150–500 mL for biogenic silica measurement were collected onto 2 µm polycarbonate membranes, and rinsed with filtered seawater. Each membrane sample was put into 15 mL centrifuge tube, dried and stored in dryers until analysis in the laboratory. The biogenic silica contents were measured by molybdenum-blue-ness spectrophotometry (Brzezinski and Nelson, 1995). Briefly, the samples were placed in a boiling water bath for 40 min, after mixed with 4 mL of 0.2 mol L^{-1} NaOH. Then the samples were cooled on ice, and neutralized with 1 mL of 1 mol L^{-1} HCl. The supernatant, obtained by centrifuging samples at 6000 × g for 10 min, were diluted with MilliQ water, and then added with 2 mL of 0.006 mol L^{-1}

ammonium molybdate and stood for 10 min. Finally, the samples were chromogenically reacted with reducing reagent for 3 h. The absorbance of samples was measured at 810 nm using a UV-VIS Spectrophotometer (DU800, Beckman, United States). For the calculation of biogenic silica contents, 0–30 μmol L^{-1} Na$_2$SiF$_6$ were used as standards.

Statistical Analyses

The statistical analysis was performed using SPSS Statistics, R and Origin. Independent-samples t-test was conducted to check the significant effects of increased pCO$_2$ at the level of $p < 0.1$, because the variations were larger within ecological replicates than biological replicates. To further detect the pCO$_2$ effects on Chl a concentration, the abundance of viruses and bacteria, BSi concentration, primary productivity and night respiration, the generalized additive mixed-effect modeling (GAMM, R packages "mgcv") was applied to analyze the data with the following procedures (Bach et al., 2017). Three GAMM models (Model I: pCO$_2$ did not affect the dependent variable, Model II: pCO$_2$ influenced the constant offset in temporal trends, Model III: pCO$_2$ changed trend shape) were fitted to each independent variable as a function of time, in which pCO$_2$ and mesocosm number were set as explanatory and random variables, respectively. To ensure model assumptions were satisfied, we considered heteroscedasticity and temporal autocorrelation of residuals, as well as autoregressive structures. The model with the highest coefficient of correlation (R^2) was defined as the best that described the pCO$_2$ effects.

RESULTS

Abiotic Environment of Mesocosms

Throughout the mesocosm experiment, most of the days were sunny, with daily mean PAR (photosynthetically active radiation) ranged 690–1075 μmol photons m^{-2} s^{-1} (**Supplementary Figure 1**). The average salinity was 30.4‰, and temperature increased gradually from 21.9 $\pm$ 0.1 to 26.1 $\pm$ 0.1°C during the period of 9th April–15th May, 2018 (**Figure 1A**).

The differences of pH$_{NBS}$, pCO$_2$ and DIC concentration between AC and HC treatments were maintained, respectively, by 0.13–0.31, 230–600 μatm, and 58–130 μmol kg^{-1} throughout the experiment ($p < 0.1$, **Figures 1B–D** and **Supplementary Table 1**). The pH$_{NBS}$ of HC and AC treatments dropped, respectively, from the initial values of 7.79 $\pm$ 0.03 and 8.01 $\pm$ 0.01, to 7.70 $\pm$ 0.05 and 7.87 $\pm$ 0.03 on day 4. Correspondingly, the DIC concentration and pCO$_2$ increased by 26 μmol kg^{-1} and 206 μatm in HC treatment, and by 41 μmol kg^{-1} and 221 μatm in AC treatments, respectively. Then the pH$_{NBS}$ increased to peak values of 7.94 $\pm$ 0.13 in HC treatments on day 10 and 8.13 $\pm$ 0.03 in AC treatments on day 12, and the corresponding DIC concentration (pCO$_2$) decreased to 1920 $\pm$ 52 μmol kg^{-1} (735 $\pm$ 246 μatm) in HC treatments and to 1824 $\pm$ 8 μmol kg^{-1} (427 $\pm$ 30 μatm) in AC treatments. Subsequently, the pH$_{NBS}$ decreased by 0.21 units in HC treatments and by 0.18 units in AC treatments on day 28, and the corresponding DIC concentration (pCO$_2$) increased by 36 μmol kg^{-1} (501 μatm)

in HC treatments and by 44 μmol kg^{-1} (263 μatm) in AC treatments. Afterward, the carbonate system of both HC and AC treatments sustained relatively stable levels till the end of the experiment.

The nutrient concentrations experienced drastic changes in the early stage of the mesocosm experiment, and maintained stable afterward (**Figure 2**). The initial concentrations of NO$_3^-$, NO$_2^-$, NH$_4^+$, PO$_4^{3-}$, and Si(OH)$_4$ in all mesocosm bags were 6.73–10.65, 0.49–0.79, 6.07–8.71, 0.18–0.47, and 5.42–9.50 μmol kg^{-1}, respectively. The concentrations of NH$_4^+$ and PO$_4^{3-}$ decreased rapidly to nearly 0 in both HC and AC treatments on day 2. However, the concentrations of NO$_3^-$, NO$_2^-$, and Si(OH)$_4$ increased at first and then decreased. The NO$_3^-$ concentration increased to 20.62 $\pm$ 14.87 μmol kg^{-1} in HC treatments and to 12.48 $\pm$ 2.77 μmol kg^{-1} in AC treatments on day 2, and then decreased dramatically to 0.10–4.73 μmol kg^{-1} on day 4. The NO$_2^-$ concentration increased up to day 2 and then maintained relatively stable till day 6, with the values of 1.99 $\pm$ 1.68 μmol kg^{-1} in HC treatments and 1.20 $\pm$ 0.38 μmol kg^{-1} in AC treatments. Subsequently, the NO$_2^-$ concentration decreased to 0.39 $\pm$ 0.48 μmol kg^{-1} in HC and to 0.44 $\pm$ 0.61 μmol kg^{-1} in AC treatments on day 8. The Si(OH)$_4$ concentration increased to 10.60 $\pm$ 2.50 μmol kg^{-1} in HC treatments and to 12.68 $\pm$ 3.03 μmol kg^{-1} in AC treatments on day 2, then decreased progressively to 1.08 $\pm$ 1.00 μmol kg^{-1} in HC and to 0.64 $\pm$ 1.28 μmol kg^{-1} in AC treatments on day 10. After reaching the very low values, the concentrations of all nutrients were stable till the end of the mesocosm experiment. No significant differences in nutrient concentrations were observed between HC and AC treatments during the whole mesocosm experiment ($p > 0.1$), except that the average concentrations of both NO$_3^-$ and NO$_2^-$ were higher ($p = 0.289$ and 0.095, respectively) in HC treatments than in AC treatments during the initial stage of the experiment.

Chlorophyll a Concentration

As shown in **Figure 3**, the temporal changes in autotrophic biomass were indicated by Chl a concentration, during the whole mesocosm experiment. The Chl a, with initial concentration of 0.17 μg L^{-1}, increased to 7.91 $\pm$ 4.02 μg L^{-1} on day 12 in AC treatments and 6.41 $\pm$ 2.80 μg L^{-1} on day 11 in HC treatments. Then it decreased to 0.91 $\pm$ 0.31 and to 1.03 $\pm$ 0.73 μg L^{-1} on day 22 in AC and HC treatments, respectively. Thereafter, Chl a concentration maintained stable till day 25 in AC treatments and to day 28 in HC treatments. Subsequently, it increased slightly to 1.34 $\pm$ 1.42 μg L^{-1} in AC treatments and to 1.00 $\pm$ 0.75 μg L^{-1} in HC treatments till the end of the experiment. Based on the ln scale of Chl a concentration, phytoplankton growth kinetics in both AC and HC treatments was classified into four phases: exponential phase (Phase I) from days 0 to 8, stationary phase (Phase II) from days 8 to 14, decline phase (Phase III) from days 12 to 25 (AC treatment) or day 28 (HC treatment), and exponential phase (Phase IV) of another growth cycle from day 25 (AC treatment) or day 28 (HC treatment) to day 31. The average value of Chl a concentration was slightly higher in HC treatments than in AC treatments during
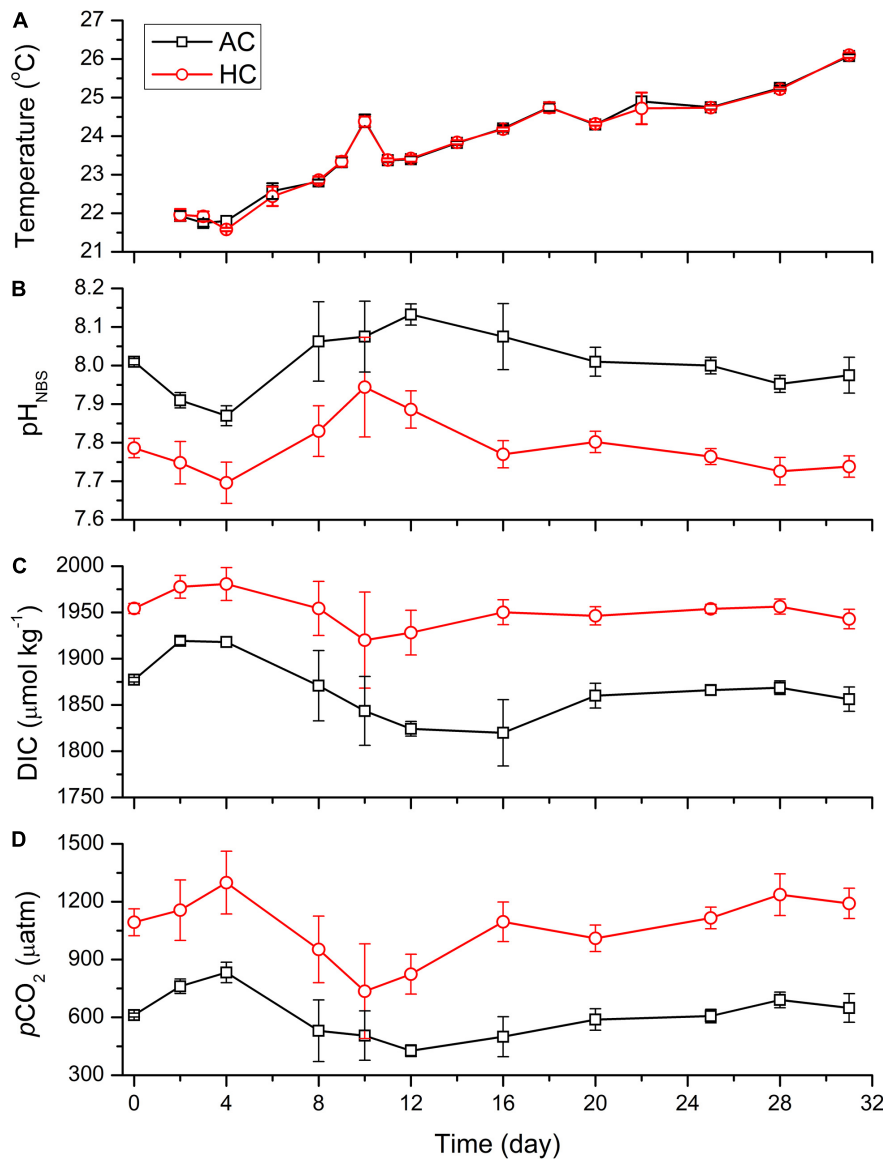
FIGURE 1 | Temporal variations of temperature **(A)**, pH_{NBS} **(B)**, DIC concentration **(C)**, and pCO_2 **(D)** in HC (1000 ppmv) and AC (∼410 ppmv) treatments. The pCO_2 was estimated from the measured pH and DIC concentration using CO2SYS program. Data are means ± SD of replicates for HC treatments and for AC treatments.

days 8–16, although the GAMM results showed that HC did not influence the development of Chl *a* concentration (**Table 1**).

Viruses and Bacteria Abundance

The abundance of viruses and bacteria underwent dynamics with different patterns, in both HC and AC treatments (**Figure 4**). The viruses abundance with initial values of 2.01–4.31 × 10⁶ particles mL⁻¹ increased, with the growth of autotrophic plankton, to 1.65 ± 0.20 × 10⁸ particles mL⁻¹ in HC treatments on day 10 and to 1.00 × 10⁸ ± 0.34 × 10⁸ particles mL⁻¹ in AC treatments on day 11, respectively. After reaching the peak, the viruses abundance decreased to 3.22 ± 0.94 × 10⁷ particles mL⁻¹ in HC treatments and to 2.70 ± 0.56 × 10⁷ particles mL⁻¹ in HC treatments on day 16. Subsequently, the viruses

abundance sustained relatively stable values till the end of the experiment in the AC treatments. In the HC treatments, however, it did not change significantly during days 16–22 but increased to 5.46 ± 2.75 × 10⁷ particles mL⁻¹ during days 25–31. The GAMM analyses revealed that elevated pCO_2 influenced the viruses trend shape (**Table 1** and **Supplementary Figure 2**), with higher abundance in HC during days 6–14 and days 25–31, relative to AC.

The initial abundance of bacteria was 1.78 ± 0.25 × 10⁶ cells mL⁻¹ in HC treatments or 1.85 ± 0.96 × 10⁶ cells mL⁻¹ in AC treatments. In the early stage of the experiment, the bacteria abundance increased rapidly to 5.94 ± 0.94 × 10⁶ cells mL⁻¹ in HC treatments on day 2, which was higher than that in AC treatments of 4.44 ± 0.54 × 10⁶ cells mL⁻¹ (p = 0.059), and then the bacteria abundance decreased till day 4 under both HC and
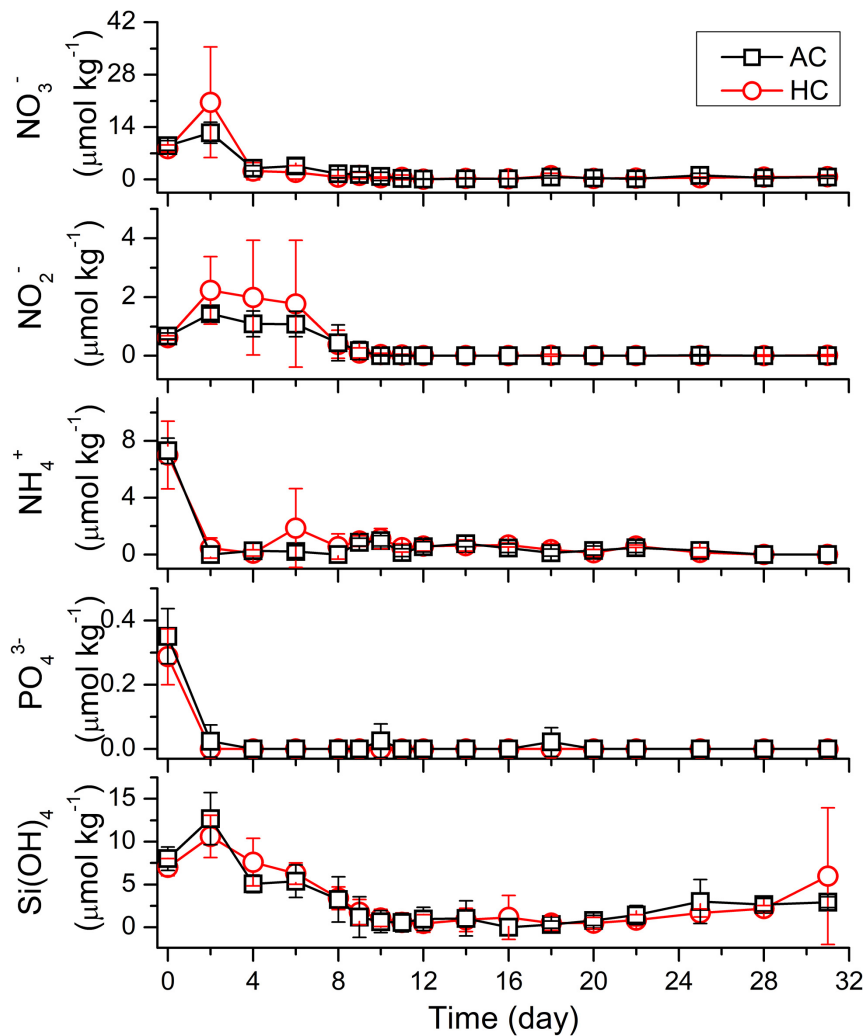
FIGURE 2 | Temporal variations of nutrients (NO_3^-, NO_2^- NH_4^+, PO_4^{3-}, and $Si(OH)_4$) in HC (1000 ppmv) and AC (~410 ppmv) treatments. Data are means ± SD of replicates for HC treatments and for AC treatments.

AC conditions. With the exponential growth of autotrophs (days 4–8), the bacteria abundance increased, however, it decreased in the stationary phase of phytoplankton (days 8–12). A constant offset in bacteria abundance existed between AC and HC, with higher bacteria abundance in HC throughout the experimental period, indicated by GAMM analyses results (**Table 1** and **Supplementary Figure 2**).

Phytoplankton Community Composition and Succession

Using microscopy, a total of 34 genera were identified, in which 26 genera belonged to diatoms and 8 genera to dinoflagellates. From all of the mesocosm bags, the dominant genera were *Chaetoceros*, *Thalassiosira*, *Rhizosolenis*, *Eucampia,* and *Prorocentrum*, and the dominant species were *Chaetoceros curvisetus*, *Rhizosolenis fragilissima*, *Eucampia zoodiacu, Cerataulina pelagica,* and *Guinardia delicatula*.

Phytoplankton community structure underwent dynamic succession at phylum levels (**Figure 5**). Diatoms accounted for a proportion of above 90% in both treatments during the period of days 0–16, subsequently decreased to 79.2 ± 13.7% in HC treatments on day 20, being higher than that of 52.2 ± 26.9% in AC treatments, although no significant differences were observed (p = 0.138). The relative abundance of diatoms appeared to decrease to 39.8 ± 28.8% in AC on day 28, but maintained stable by 81.8 ± 14.5% in HC treatments, resulting in more significant differences in relative abundance of diatoms between HC and AC treatments (p = 0.054). Correspondingly, dinoflagellates dominated by *Prorocentrum minimum* and *Peridinium conicoides*, maintained relatively stable abundance with variations less than 10% in HC treatments, but increased to 60.2 ± 28.8% in AC treatments.

The dynamic changes of community structure were more complicated at genus and species levels than at phylum level (**Figure 6** and **Supplementary Figure 3**). The diatom *Guinardia,*

FIGURE 3 | Temporal variations of Chl *a* concentration **(A)** and the ln scale of Chl *a* concentration **(B)** in HC (1000 ppmv) and AC (∼410 ppmv) treatments. Data are means ± SD of replicates for HC treatments and for AC treatments.
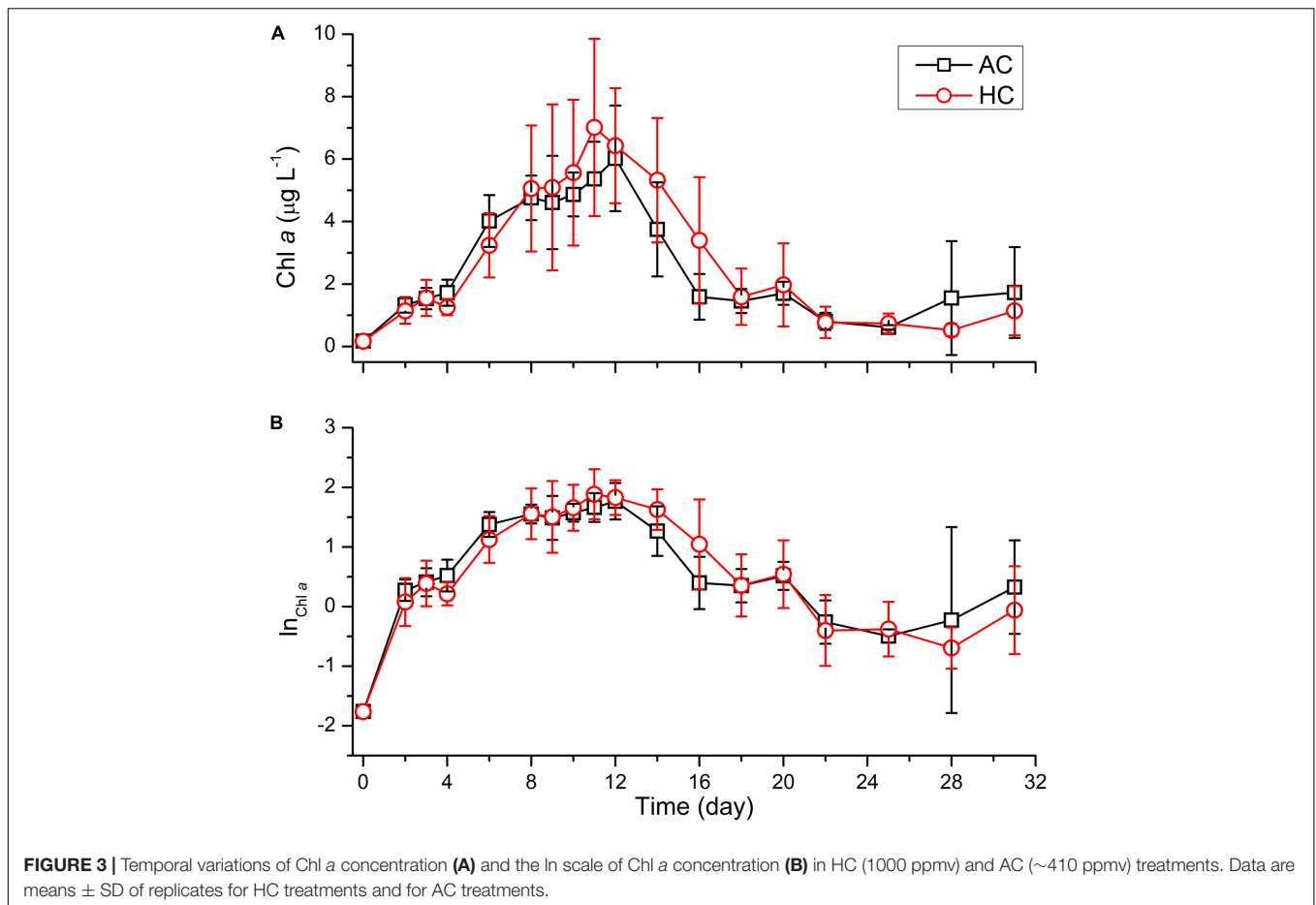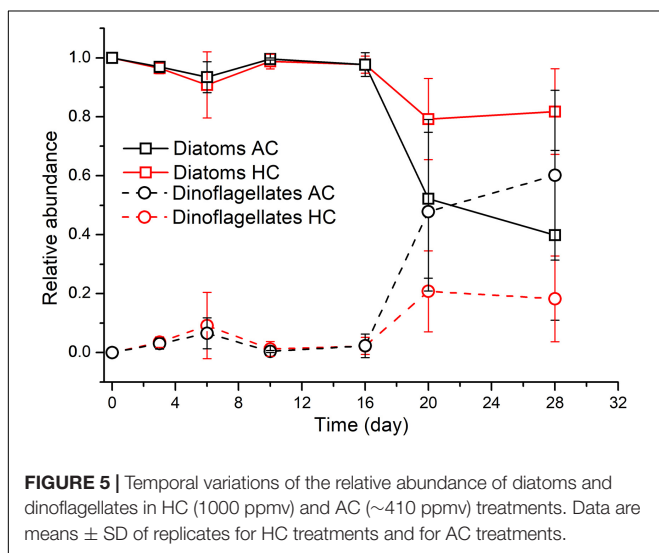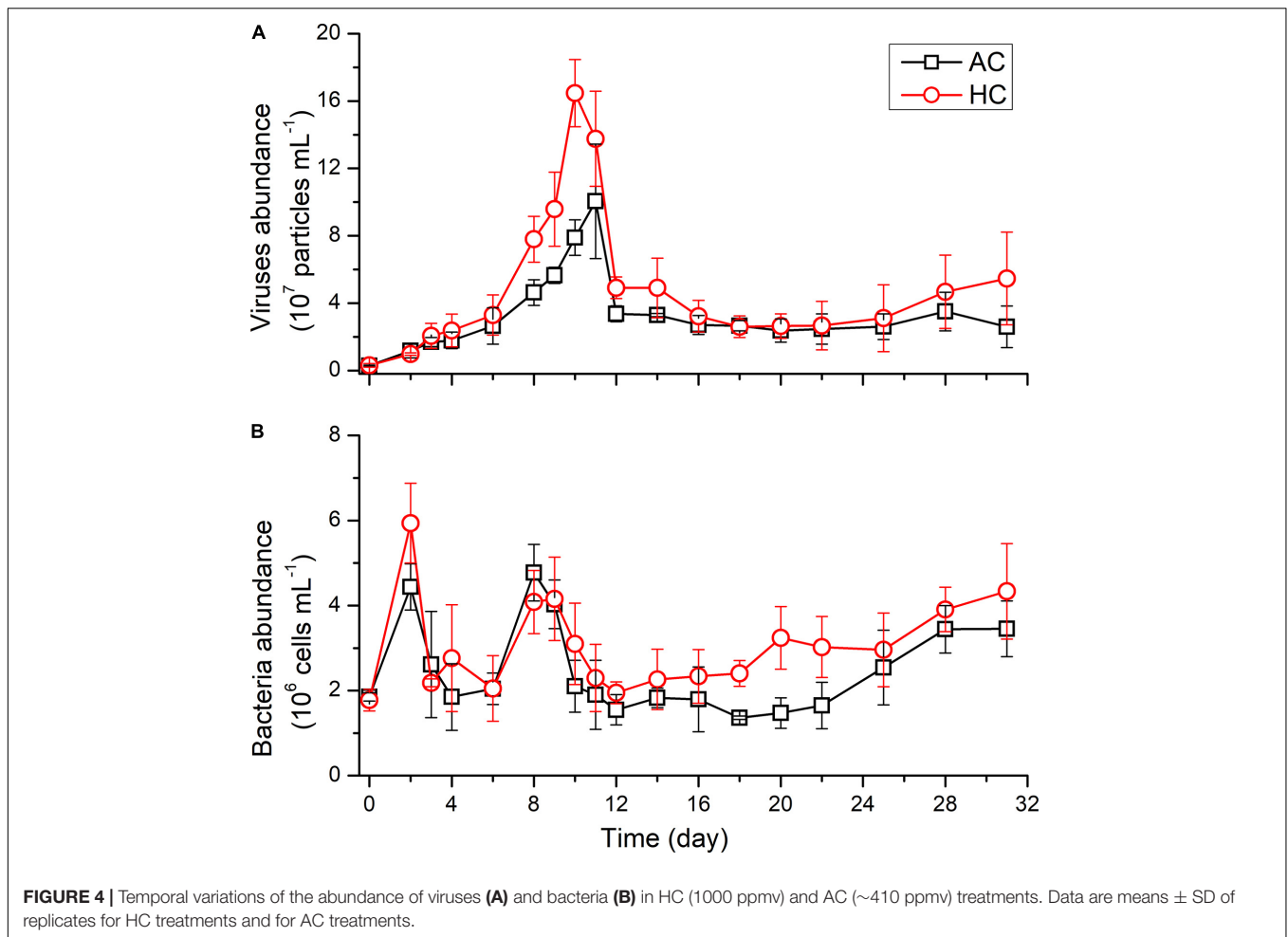
TABLE 1 | The GAMM analyses results of Chl *a* concentration, the abundance of viruses and bacteria, BSi concentration, primary productivity and night respiration.

Dependent variables	pCO_2 effects	R^2	Temporal autocorrelation	Autoregressive structure	Remark
Chl *a* concentration	type A	0.497	Yes	second order	
Bacteria abundance	type B	0.601	No	0	
Viruses abundance	type C	0.850	No	0	
Day-time primary productivity	type A	0.717	No	0	Chl *a* was added as explanatory variable
Daily net primary productivity	type A	0.642	No	0	Chl *a* was added as explanatory variable
Night-period respiration	type A	0.406	No	0	Chl *a* was added as explanatory variable
BSi concentration	type A	0.739	Yes	0	Temporal autocorrelation could not be resolved

The pCO_2 effects were classified into three types (type A: pCO_2 did not affect the dependent variable, type B: pCO_2 influenced the constant offset in temporal trends, and type C: pCO_2 changed trend shape).

dominated by *G. delicatula*, was the most abundant with relative abundance of 53.4% in terms of total diatom + dinoflagellate species, with cell density of about 9.9×10^4 cells mL^{-1}, after *in situ* community was inoculated into mesocosm bags. However, it decreased rapidly to average relative abundance of 3.2% (density of 2.6×10^3 cells mL^{-1}) and to 1.0% (density of 1.6×10^3 cells mL^{-1}) on day 3 in AC and HC treatments, respectively, and no longer existed from day 6. The diatom *Eucampia* in both HC and AC treatments, mainly composed of *E. zoodiacu*, maintained density of approximately 6×10^4– 9×10^4 cells mL^{-1} during days 0–16, then dropped to 0.2×10^4–3.7×10^4 cells mL^{-1} on day 20 and maintained

stable afterward. The relative abundance of *Eucampia* increased from initial value of 29% to 61–76% and to 71–75% during days 3–6, and subsequently decreased to 7–16% and to 1–13% on day 10, in HC and AC treatments, respectively. The diatom *Chaetoceros* grew exponentially from 1.4×10^4 cells mL^{-1}, and reached the peak on day 10 with average concentration of 2.9×10^6 cells mL^{-1} in HC and 3.4×10^6 cells mL^{-1} in AC treatments, which accounted for 65.3 and 71.9% of diatom + dinoflagellate assemblages, respectively. Subsequently, the dominant genus in both HC and AC treatments became the diatom *Thalassiosira* and *Rhizosolenis* with the average relative abundance of 53 and 34% on day 16, respectively.

FIGURE 4 | Temporal variations of the abundance of viruses **(A)** and bacteria **(B)** in HC (1000 ppmv) and AC (~410 ppmv) treatments. Data are means ± SD of replicates for HC treatments and for AC treatments.

FIGURE 5 | Temporal variations of the relative abundance of diatoms and dinoflagellates in HC (1000 ppmv) and AC (~410 ppmv) treatments. Data are means ± SD of replicates for HC treatments and for AC treatments.

Then the abundance of *Thalassiosira* and *Rhizosolenis* decreased progressively. During the late stage of these experiment, HC stimulated the growth of the diatom *Nitzschia* on day 20, but
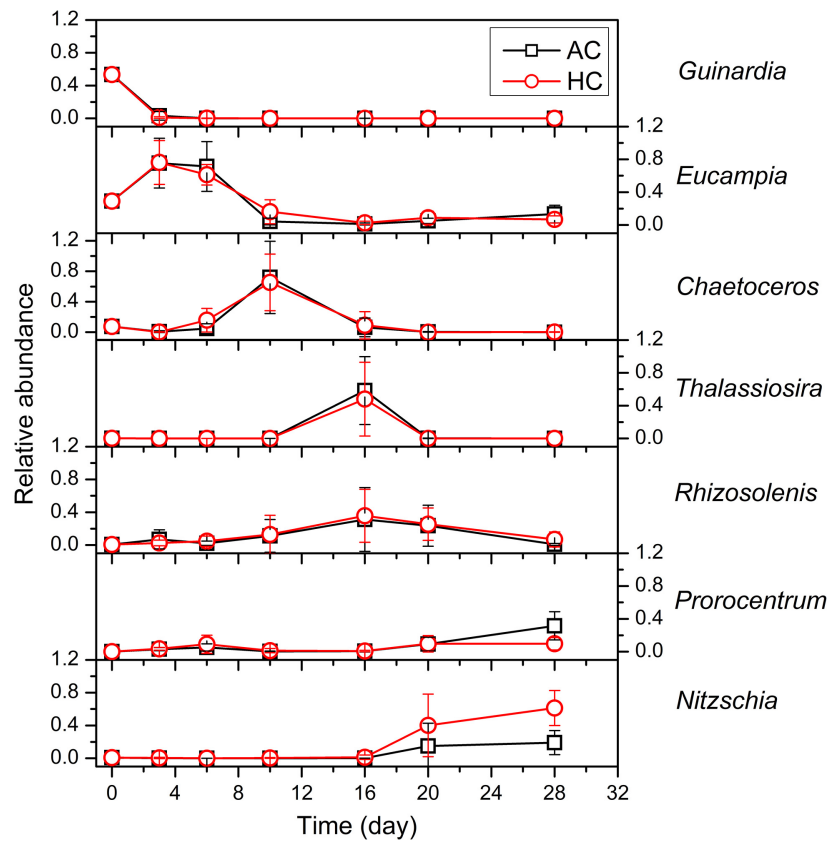
AC stimulated the growth of the dinoflagellate *Propocentrum* on day 28. As a consequence, the diatom *Nitzschia* had significantly higher relative abundance during days 20–28 (p = 0.019), with the dinoflagellate *Propocentrum* accounting for lower proportion on day 28 (p = 0.078), in HC relative to AC treatments.

Primary Productivity and Night-Period Respiration

The temporal variations of day-time primary productivity, daily net primary productivity and night respiratory carbon loss normalized to water volume showed similar changing patterns with autotrophic biomass levels indicated by Chl a concentration (**Figure 7**). The day-time primary productivity and daily net primary productivity increased with the growth of phytoplankton, from initial values of 24–77 and 21–63 µg C L^{-1}, to the peak values of 573 and 392 µg C L^{-1} on average, respectively, as Chl a concentration reached the maximum. Subsequently, the day-time primary productivity and daily net primary productivity decreased progressively, with the decay of algal blooms, with lowered values of 6.5–204 and 6.3–111 µg C L^{-1} after day 22. Respiration carbon loss of phytoplankton during night period increased from 15 µg C L^{-1}

FIGURE 6 | The succession of the dominant phytoplankton at genus level in HC (1000 ppmv) and AC (∼410 ppmv) treatments. Data are means ± SD of replicates for HC treatments and for AC treatments.

on average during days 2–8 to 150 μg C L⁻¹ on average on day 9. Subsequently, the night period respiration of phytoplankton maintained a rate of 140–180 μg C L⁻¹ during the stationary phase of autotrophs, and decreased progressively with the decline of autotrophic blooms. Finally, the respiration stayed 7–9 μg C L⁻¹ during days 22–28, and increased slightly at the end of the mesocosm experiment. The daily net primary productivity and day-time primary productivity normalized to Chl *a* increased immediately from the initial values of 17.3 ± 4.0 and 26.8 ± 9.6 μg C (μg Chl *a*)⁻¹, to 88.7 ± 23.9 and 100.1 ± 30.3 μg C (μg Chl *a*)⁻¹ on day 6, and then sustained relatively stable levels with the average values of 48.2 and 67.9 μg C (μg Chl *a*)⁻¹. The night-period respiration normalized to Chl *a*, with lower values of 12.3 μg C (μg Chl *a*)⁻¹ during days 0–9, increased drastically and maintained higher values of 12.3 μg C (μg Chl *a*)⁻¹. Neither primary productivity nor night respiration of phytoplankton was influenced significantly by HC (**Table 1**), normalized to water volume or to Chl *a*, at any time points examined during the experiment.
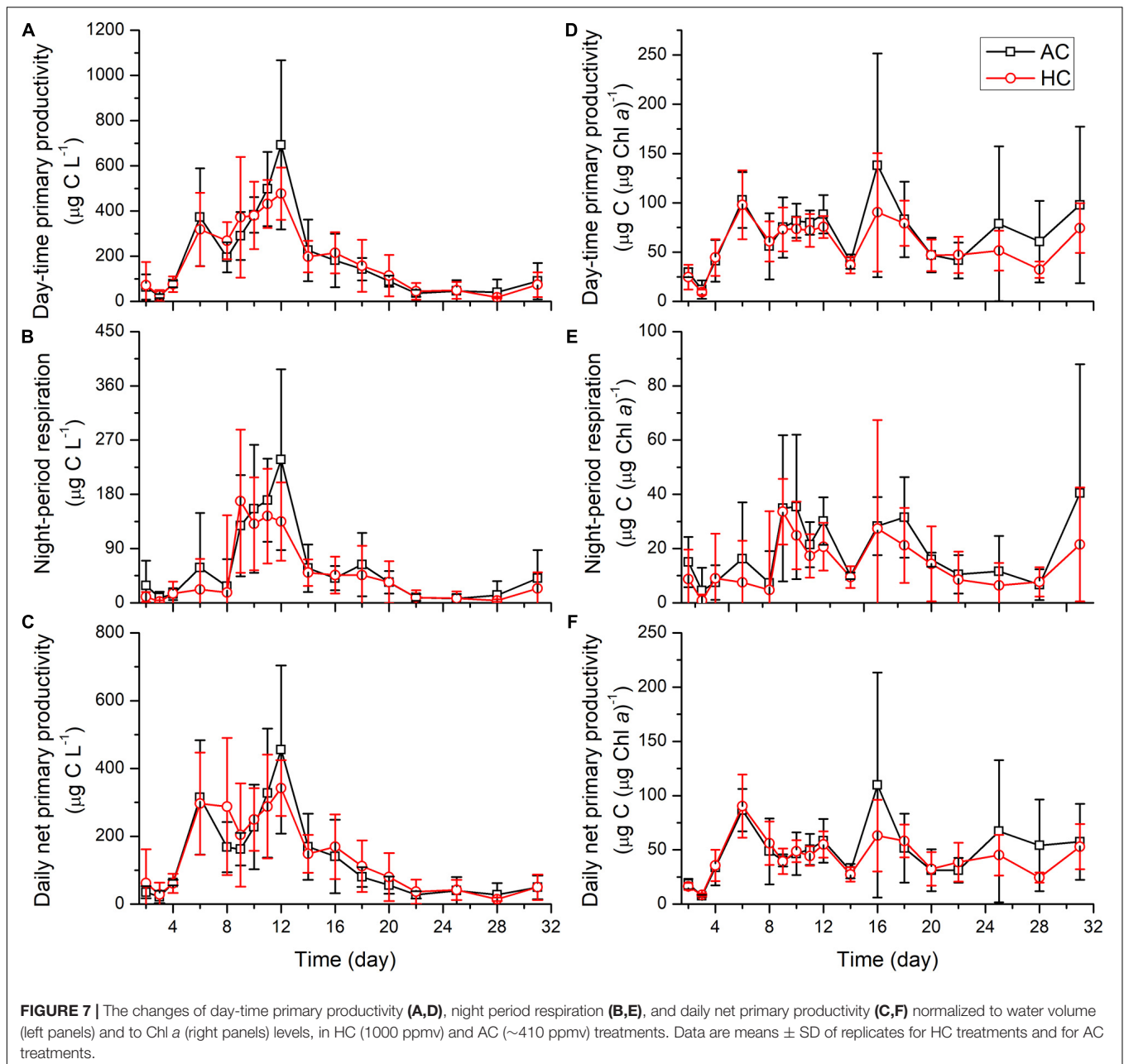
Biogenic Silica Contents
Throughout the mesocosm experiment, the differences in temporal development of biogenic silica (BSi) contents were not observed between HC and AC treatments (**Table 1** and

Figure 8). With development of phytoplankton blooms, the BSi concentration in the water increased and reached peak values of 11.3 ± 0.5 μmol BSi L⁻¹ on day 12. Correspondingly, the BSi contents normalized to Chl *a* increased from the initial values of approximately 0.05–2.1 ± 0.8 μmol BSi (μg Chl *a*)⁻¹ on day 4, and then maintained relative stable till day 14. Afterward, the BSi concentration in the water decreased, while the BSi contents normalized to Chl *a* increased, with the decay of phytoplankton blooms till the end of the experiment.
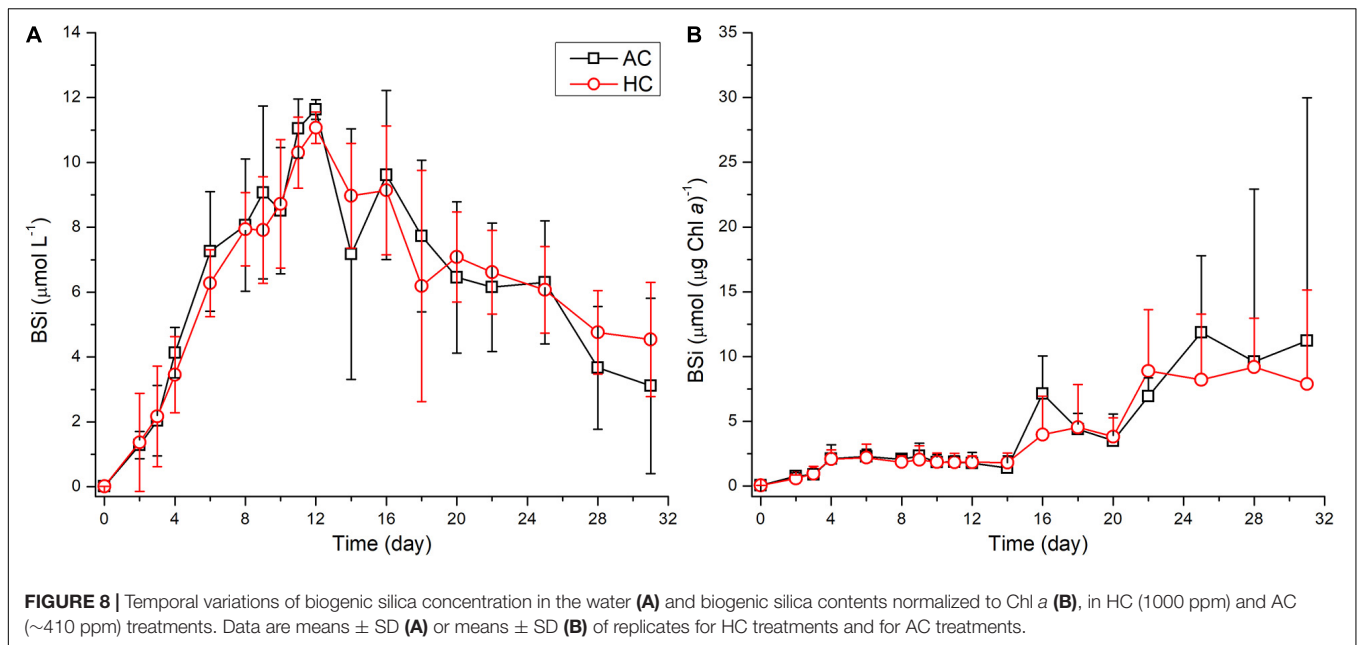
DISCUSSION

The results from our mesocosm experiment during the period of late spring and early summer indicate that elevated CO₂ concentration to the level projected for the end of this century, along with natural rise of surface seawater temperature, altered phytoplankton community structure, with impeded succession from diatoms to dinoflagellates and enhanced abundance of free-living viruses and heterotrophic bacteria. Such an ecological response may lead to significant changes in biogeochemical cycles of carbon and nutrients.

The succession from diatoms to dinoflagellates occurred after diatom blooms declined (**Figures 5**, **6**). Under the ambient CO₂ level, the dominant diatom *Nitzschia closterium* was replaced by

FIGURE 7 | The changes of day-time primary productivity **(A,D)**, night period respiration **(B,E)**, and daily net primary productivity **(C,F)** normalized to water volume (left panels) and to Chl a (right panels) levels, in HC (1000 ppmv) and AC (~410 ppmv) treatments. Data are means ± SD of replicates for HC treatments and for AC treatments.

the mixotrophic dinoflagellates *P. minimum* and *P. conicoides*. The phenomenon of succession from diatoms to dinoflagellates have been commonly observed in eutrophic coastal regions (Spilling et al., 2018), which appears to be due to different physiological strategies between the two groups in coping with environmental changes, including CO_2 and temperature changes. It is most likely that mixotrophic dinoflagellates take over the dominance by taking up organic matters after diatoms depleted the inorganic nutrients (Carlsson and Granéli, 1998). Alternatively, dinoflagellates may possess positive interaction with surrounding bacteria consortia to exchange and/or consume matters (Gong et al., 2017). In addition, the heterotrophic metabolism and flagellate motility may boost with increasing

temperature. In the present work, water temperature increased by 4.2°C from 21.9 ± 0.1°C at the beginning to 26.1 ± 0.1°C at the end of the experiment (**Figure 1A**). Notably, the competitive capacity of dinoflagellates might become lower in the mesocosms relative to the bay, resulting from low abundance and diversity of dinoflagellates in the bay when the mesocosm experiment was initiated, and from suboptimal growth conditions for dinoflagellates in the mesocosms such as aeration disturbance (Lin et al., 2012; Wohlrab et al., 2020). We also noted that the composition of diatoms changed, with larger cells tending to account for higher proportion (**Figure 6**, Olenina, 2006; Bach et al., 2019). This observation seemed contradict to the strategy of diatoms in coping with nutrients limitation and increasing

FIGURE 8 | Temporal variations of biogenic silica concentration in the water **(A)** and biogenic silica contents normalized to Chl a **(B)**, in HC (1000 ppm) and AC (~410 ppm) treatments. Data are means ± SD **(A)** or means ± SD **(B)** of replicates for HC treatments and for AC treatments.

temperature, which usually results in smaller cells become the dominant (Finkel et al., 2010; Barton et al., 2013). However, larger diatoms have the advantages of storing nutrient for slower growth (Raven, 1987), and heterotrophic refueling of nutrients may also contribute the increased proportion of larger diatoms.

Under the elevated CO_2 concentration, however, the succession of phytoplankton from diatoms to dinoflagellates appeared to occur, but to much less extent, which was not enough for the latter to replace the former for the dominant group (**Figures 5**, **6**). Higher relative abundance of diatoms under HC conditions was also observed in KOSMOS mesocosm experiment conducted in the Gulmar Fjord, Sweden (Bach et al., 2017), as well as at Shikine Island CO_2 seep, Japan (Harvey et al., 2019; Wada et al., 2021). These may attribute to competitive advantages of CCMs in diatoms, under HC conditions. Increased CO_2 availability associated with ocean acidification can fuel phytoplankton biomass when CO_2 becomes limited (Hansen et al., 2007; Berge et al., 2010; Raven et al., 2020). While increased CO_2 levels projected to the end of this century have been shown to down-regulate CCMs in diatoms (see the review by Gao and Campbell, 2014 and literatures therein) and in dinoflagellates (Rost et al., 2006), and the saved energy from operation of CCMs may be beneficial or harmful to phytoplankton growth under limiting and inhibiting light levels, respectively (Gao et al., 2012). Therefore, difference in CCMs efficiency between the two groups might be responsible for the suppressed succession from diatoms to dinoflagellates under the HC. The CO_2 affinity of ribulose 1,5-diphosphate carboxylase/oxidase (Rubisco) for carboxylation is higher in diatoms than dinoflagellates (Reinfelder, 2011). Dinoflagellates possess a high plasticity toward increased pCO_2, while diatoms do not (Van de Waal et al., 2019). Considering the higher CO_2 affinity and lack of CCMs plasticity, diatoms may gain a competitive advantage in DIC uptake under elevated pCO_2 conditions. In addition, OA

effects on phytoplankton can be modified by other abiotic factors such as temperature and nutrients, depending on taxa and latitude or weather conditions, and therefore would influence plankton community structure (Sommer et al., 2015; Bach et al., 2016). Diatoms migrated poleward more slowly relative to dinoflagellates, implying that diatoms are more resilient to ocean warming (Chivers et al., 2017), and that diatoms would gain more advantages under OA conditions with increasing temperature. Algal responses to nutrient enrichment may differ at small and intermediate mesocosm volumes but are similar in larger volume mesocosms (>20 L), which are typically used in field (Spivak et al., 2011). Therefore, our experiment with a natural community in >3000 L mesocosm had been performed under different levels of CO_2 could provide basic understanding of the OA impacts on natural plankton communities in eutrophic regions. A previous study showed that plankton communities supported by regenerated nutrients may be more responsive to OA than those having access to higher availability of inorganic nutrients (Bach et al., 2016). Under HC conditions, the dominant diatoms *Nitzschia* spp. have a benefit in nutrient uptake (Qu et al., 2017), and less resources were necessary for diatom inorganic carbon acquisition (Bach et al., 2017). Therefore, elevated pCO_2 along with depletion of nutrients hindered the takeover by dinoflagellates, though a meta-analysis study showed that elevated CO_2 appears to favor dinoflagellates more than diatoms in terms of growth (Seifert et al., 2020). On the other hand, increased bacteria and viruses abundance under HC (**Figure 4**), along with boosted bacterial activity by high temperature (Spilling et al., 2018), could release more nutrients and CO_2 due to enhanced degradation of organic matters, though the inorganic macro-nutrients did not differ obviously (**Figure 2**).

Throughout processes of phytoplankton blooms, higher autotrophic biomass was observed in HC relative to AC, but the

difference was not significant (**Figure 3**). The rapid increase in phytoplankton biomass led to the quick declines in nutrients from days 2 to 4. Phytoplankton biomass continued to increase even when the levels of NO_3^- and PO_4^{3-} were very low. This process may be supported by the degradation of organic matters driven by bacteria, as indicated by increased concentrations of NO_x^- and $Si(OH)_4$, decreased NH_4^+ concentration and increased bacteria abundance on day 2 (**Figure 2**). At the early stage, higher NO_x^- concentration and higher bacteria abundance in HC relative to AC treatments, indicated that OA stimulated more nutrient refueling by bacterial nitrification to support higher phytoplankton biomass. However, the abundances of viruses and bacteria were increased by HC during the growing and declining phase of phytoplankton, respectively, implying that the enhancement of cell lysis by viruses and the negative interaction of bacteria with diatoms (Vincent and Bowler, 2020) may offset the positive effects of OA on autotrophic biomass. In addition, phytoplankton biomass in HC reached the peak one day earlier than AC, which could be attributed to faster exhaustion of nutrients with higher biomass in HC.

While phytoplankton community structure and abundances of viruses and bacteria responded to the elevated pCO$_2$, no significant changes were observed in primary productivity of phytoplankton assemblages over time, either normalized to water volume or to Chl a (**Figure 7**). High pCO$_2$ also did not significantly influence the production or degradation of BSi (**Figure 8**). Changes in the milieu pH could affect intracellular acid-base homeostasis, which in turn influences silicon metabolism, expansion of vesicle expansion and valve formation (Hervé et al., 2012). In this study, the initial pCO$_2$ of seawater in AC cultures was 610 µatm, which was higher than that equilibrated with ambient air pCO$_2$ of about 410 ppmv. This indicated that eutrophication contributed strongly to the CO$_2$ enrichment and acidification, with a pH drop of 0.15 units. In addition, phytoplankton in this region have adapted to fluctuating pH with 0.11–0.18 units of daily ∆pH, due to high rates of day-time photosynthetic CO$_2$ removal and night-time respiratory CO$_2$ release. Non-significant effects of HC on primary productivity and BSi contents may result from high resilience of phytoplankton physiological performance to OA and/or balanced effects of elevated pCO$_2$ and increased acidic stress (Gao et al., 2019). Although differences in primary productivity or BSi contents were not observed between HC and AC treatments, OA could influence biogeochemical cycles of carbon and nutrients because of varied plankton community structure. BSi contents normalized to Chl a maintained stable during the processes of bloom development, but increased with the decline of phytoplankton blooms, reflecting lower rates of BSi remineralizatin by bacteria relative to phytoplankton mortality rates.

In conclusion, our mesocosm experiment demonstrated a community level response to the elevated CO$_2$ in the eutrophic bay in the coastal waters of the East China Sea, showing repressed species succession of phytoplankton from diatoms to dinoflagellates and enhanced abundance of viruses and heterotrophic bacteria. This finding mirrors observed reduction in biodiversity near shallow CO$_2$ seeps (Cigliano et al., 2010; Hall-Spencer and Harvey, 2019; Harvey et al., 2021), since acidification would eventually result in "winners" and "losers" (Gattuso et al., 2015). Although we only found that bacteria increased their abundance, it is most likely that their community structure changed, since OA enhanced nitrification at the early stage. The altered bacterial communities by OA were also shown in the waters surrounding a CO$_2$ seep (Harvey et al., 2020). Increased viruses abundance suggested that OA may enhance viral activity, as shown previously that elevated CO$_2$ exacerbates viruses attack to its host, a red-tide microalga (Chen et al., 2015). Integratively, OA may alter phytoplankton succession and enhance viral lysis and bacterial degradation, consequently alter biogeochemical processes in eutrophic coastal ecosystems.

DATA AVAILABILITY STATEMENT

The raw data supporting the conclusions of this article will be made available by the authors, without undue reservation.

AUTHOR CONTRIBUTIONS

KG, XL, and GG designed the experiment. TW, XY, DZ, JS, SC, HL, NB, RH, LQ, and XJ preserved normal operation of the mesocosm platform. JS, RH, and SC measured pH, salinity, temperature, primary productivity, and biogenic silica contents. XJ and LQ measured chlorophyll a concentration. ZW and YG provided phytoplankton community structure. YY, RZ, and NJ provided viruses and bacteria abundance. XS provided the concentration of nutrient and dissolved inorganic carbon. RH wrote the manuscript. All authors revised the manuscript.

FUNDING

ACKNOWLEDGMENTS

SUPPLEMENTARY MATERIAL

The Supplementary Material for this article can be found online at: https://www.frontiersin.org/articles/10.3389/fmars.2021.642208/full#supplementary-material

REFERENCES

Aberle, N., Schulz, K. G., Stuhr, A., Malzahn, A. M., Ludwig, A., and Riebesell, U. (2013). High tolerance of microzooplankton to ocean acidification in an Arctic coastal plankton community. *Biogeosciences* 10, 1471–1481. doi: 10.5194/bg-10-1471-2013

Bach, L. T., Alvarez-Fernandez, S., Hornick, T., Stuhr, A., and Riebesell, U. (2017). Simulated ocean acidification reveals winners and losers in coastal phytoplankton. *PLoS One* 12:e0188198. doi: 10.1371/journal.pone.0188198

Bach, L. T., Hernández-Hernández, N., Taucher, J., Spisla, C., Sforna, C., Riebesell, U., et al. (2019). Effects of elevated CO_2 on a natural diatom community in the subtropical NE Atlantic. *Front. Mar. Sci.* 6:75. doi: 10.3389/fmars.2019.00075

Bach, L. T., Taucher, J., Boxhammer, T., Ludwig, A., Kristineberg KOSMOS Consortium, Achterberg, E. P., et al. (2016). Influence of ocean acidification on a natural winter-to-summer plankton succession: first insights from a long-term mesocosm study draw attention to periods of low nutrient concentrations. *PLoS One* 11:e0159068. doi: 10.1371/journal.pone.0159068

Barton, A. D., Finkel, Z. V., Ward, B. A., Johns, D. G., and Follows, M. J. (2013). On the roles of cell size and trophic strategy in North Atlantic diatom and dinoflagellate communities. *Limnol. Oceanogr.* 58, 254–266. doi: 10.4319/lo.2013.58.1.0254

Berge, T., Daugbjerg, N., Balling Andersen, B., and Hansen, P. J. (2010). Effect of lowered pH on marine phytoplankton growth rates. *Mar. Ecol. Prog. Ser.* 416, 79–91. doi: 10.3354/meps08780

Brzezinski, M. A., and Nelson, D. M. (1995). The annual silica cycle in the Sargasso Sea near Bermuda. *Deep Sea Res. I Oceanogr. Res. Papers* 42, 1215–1237. doi: 10.1016/0967-0637(95)93592-3

Cai, W.-J., Hu, X., Huang, W.-J., Murrell, M. C., Lehrter, J. C., Lohrenz, S. E., et al. (2011). Acidification of subsurface coastal waters enhanced by eutrophication. *Nat. Geosci.* 4, 766–770. doi: 10.1038/ngeo1297

Carlsson, P., and Granéli, E. (1998). "Utilization of dissolved organic matter (DOM) by phytoplankton including harmful species," in *Physiological Ecology of Harmful Algal Blooms*, eds M. A. Donald and D. C. Allan (Heidelberg: Springer), 509–524.

Chen, S., Gao, K., and Beardall, J. (2015). Viral attack exacerbates the susceptibility of a bloom-forming alga to ocean acidification. *Glob. Change Biol.* 21, 629–636. doi: 10.1111/gcb.12753

Chen, X., Wei, W., Wang, J., Li, H., Sun, J., Ma, R., et al. (2019). Tide driven microbial dynamics through virus-host interactions in the estuarine ecosystem. *Water Res.* 160, 118–129. doi: 10.1016/j.watres.2019.05.051

Chivers, W. J., Walne, A. W., and Hays, G. C. (2017). Mismatch between marine plankton range movements and the velocity of climate change. *Nat. Commun.* 8:14434. doi: 10.1038/ncomms14434

Cigliano, M., Gambi, M. C., Rodolfo-Metalpa, R., Patti, F. P., and Hall-Spencer, J. M. (2010). Effects of ocean acidification on invertebrate settlement at volcanic CO_2 vents. *Mar. Biol.* 157, 2489–2502. doi: 10.1007/s00227-010-1513-6

de Kluijver, A., Soetaert, K., Czerny, J., Schulz, K. G., Boxhammer, T., Riebesell, U., et al. (2013). A ^{13}C labelling study on carbon fluxes in Arctic plankton communities under elevated CO_2 levels. *Biogeosciences* 10, 1425–1440. doi: 10.5194/bg-10-1425-2013

Engel, A., Zondervan, I., Aerts, K., Beaufort, L., Benthien, A., Chou, L., et al. (2005). Testing the direct effect of CO_2 concentration on a bloom of the coccolithophorid *Emiliania huxleyi* in mesocosm experiments. *Limnol. Oceanogr.* 50, 493–507. doi: 10.4319/lo.2005.50.2.0493

Finkel, Z. V., Beardall, J., Flynn, K. J., Quigg, A., Rees, T. A. V., and Raven, J. A. (2010). Phytoplankton in a changing world: cell size and elemental stoichiometry. *J. Plankton Res.* 32, 119–137. doi: 10.1093/plankt/fbp098

Friedlingstein, P., O'Sullivan, M., Jones, M. W., Andrew, R. M., Hauck, J., Olsen, A., et al. (2020). Global carbon budget 2020. *Earth Syst. Sci. Data* 12, 3269–3340. doi: 10.5194/essd-12-3269-2020

Gao, K., Beardall, J., Häder, D.-P., Hall-Spencer, J. M., Gao, G., and Hutchins, D. A. (2019). Effects of ocean acidification on marine photosynthetic organisms under the concurrent influences of warming, UV radiation, and deoxygenation. *Front. Mar. Sci.* 6:322. doi: 10.3389/fmars.2019.00322

Gao, K., and Campbell, D. A. (2014). Photophysiological responses of marine diatoms to elevated CO_2 and decreased pH: a review. *Funct. Plant Biol.* 41, 449–459. doi: 10.1071/FP13247

Gao, K., Xu, J., Gao, G., Li, Y., Hutchins, D. A., Huang, B., et al. (2012). Rising CO_2 and increased light exposure synergistically reduce marine primary productivity. *Nat. Clim. Chang.* 2, 519–523. doi: 10.1038/nclimate1507

Gattuso, J.-P., Magnan, A., Billé, R., Cheung, W. W. L., Howes, E. L., Joos, F., et al. (2015). Contrasting futures for ocean and society from different anthropogenic CO_2 emissions scenarios. *Science* 349:aac4722. doi: 10.1126/science.aac4722

Gong, W., Browne, J., Hall, N., Schruth, D., Paerl, H., and Marchetti, A. (2017). Molecular insights into a dinoflagellate bloom. *ISME J.* 11, 439–452. doi: 10.1038/ismej.2016.129

Hall-Spencer, J. M., and Harvey, B. P. (2019). Ocean acidification impacts on coastal ecosystem services due to habitat degradation. *Emerg. Top. Life Sci.* 3, 197–206. doi: 10.1042/ETLS20180117

Hansen, P. J., Lundholm, N., and Rost, B. (2007). Growth limitation in marine red-tide dinoflagellates: effects of pH versus inorganic carbon availability. *Mar. Ecol. Prog. Ser.* 334, 63–71. doi: 10.3354/meps334063

Hare, C. E., Leblanc, K., DiTullio, G. R., Kudela, R. M., Zhang, Y., Lee, P. A., et al. (2007). Consequences of increased temperature and CO_2 for phytoplankton community structure in the Bering Sea. *Mar. Ecol. Prog. Ser.* 352, 9–16. doi: 10.3354/meps07182

Harvey, B., Agostini, S., Kon, K., Wada, S., and Hall-Spencer, J. (2019). Diatoms dominate and alter marine food-webs when CO_2 rises. *Diversity* 11:242. doi: 10.3390/d11120242

Harvey, B. P., Kerfahi, D., Jung, Y., Shin, J.-H., Adams, J. M., and Hall-Spencer, J. M. (2020). Ocean acidification alters bacterial communities on marine plastic debris. *Mar. Pollut. Bull.* 161:111749. doi: 10.1016/j.marpolbul.2020.111749

Harvey, B. P., Kon, K., Agostini, S., Wada, S., and Hall-Spencer, J. M. (2021). Ocean acidification locks algal communities in a species-poor early successional stage. *Glob. Change Biol.* 27, 2174–2187. doi: 10.1111/gcb.15455

Hervé, V., Derr, J., Douady, S., Quinet, M., Moisan, L., and Lopez, P. J. (2012). Multiparametric analyses reveal the pH-dependence of silicon biomineralization in diatoms. *PLoS One* 7:e46722. doi: 10.1371/journal.pone.0046722

IPCC (2019). *Special Report on the Ocean and Cryosphere in a Changing Climate.* Geneva: IPCC.

Lewis, E., and Wallace, D. (1998). *Program Developed for CO_2 System Calculations.* Berkeley, CA: Environmental System Science Data Infrastructure for a Virtual Ecosystem (ESS-DIVE) (United States).

Lin, G., Yang, Q., Lin, W., and Wang, Y. (2012). Distribution characteristic and variation trend of planktonic dinoflagellate in the Taiwan Strait from 2006 to 2007. *Mar. Sci. Bull.* 14, 68–79.

Lin, X., Huang, R., Li, Y., Li, F., Wu, Y., Hutchins, D. A., et al. (2018). Interactive network configuration maintains bacterioplankton community structure under elevated CO_2 in a eutrophic coastal mesocosm experiment. *Biogeosciences* 15, 551–565. doi: 10.5194/bg-15-551-2018

Liu, N., Tong, S., Yi, X., Li, Y., Li, Z., Miao, H., et al. (2017). Carbon assimilation and losses during an ocean acidification mesocosm experiment, with special reference to algal blooms. *Mar. Environ. Res.* 129, 229–235. doi: 10.1016/j.marenvres.2017.05.003

Meakin, N. G., and Wyman, M. (2011). Rapid shifts in picoeukaryote community structure in response to ocean acidification. *ISME J.* 5, 1397–1405. doi: 10.1038/ismej.2011.18

Niehoff, B., Schmithüsen, T., Knüppel, N., Daase, M., Czerny, J., and Boxhammer, T. (2013). Mesozooplankton community development at elevated CO_2 concentrations: results from a mesocosm experiment in an Arctic fjord. *Biogeosciences* 10, 1391–1406. doi: 10.5194/bg-10-1391-2013

Olenina, I. (2006). Biovolumes and size-classes of phytoplankton in the Baltic Sea. *HELCOM Balt. Sea Environ. Proc.* 106:144.

Qu, C.-F., Liu, F.-M., Zheng, Z., Wang, Y.-B., Li, X.-G., Yuan, H.-M., et al. (2017). Effects of ocean acidification on the physiological performance and carbon production of the Antarctic sea ice diatom *Nitzschia* sp. ICE-H. *Mar. Pollut. Bull.* 120, 184–191. doi: 10.1016/j.marpolbul.2017.05.018

Rabalais, N. N., Turner, R. E., Díaz, R. J., and Justić, D. (2009). Global change and eutrophication of coastal waters. *ICES J. Mar. Sci.* 66, 1528–1537. doi: 10.1093/icesjms/fsp047

Raven, J. A. (1987). The role of vacuoles. *New Phytol.* 106, 357–422.

Raven, J. A., Gobler, C. J., and Hansen, P. J. (2020). Dynamic CO_2 and pH levels in coastal, estuarine, and inland waters: theoretical and observed effects on harmful algal blooms. *Harmful Algae* 91:101594. doi: 10.1016/j.hal.2019.03.012

Reinfelder, J. R. (2011). Carbon concentrating mechanisms in eukaryotic marine phytoplankton. *Annu. Rev. Mar. Sci.* 3, 291–315. doi: 10.1146/annurev-marine-120709-142720

Riebesell, U., Aberle-Malzahn, N., Achterberg, E. P., Algueró-Muñiz, M., Alvarez-Fernandez, S., Arístegui, J., et al. (2018). Toxic algal bloom induced by ocean acidification disrupts the pelagic food web. *Nat. Clim. Chang.* 8, 1082–1086. doi: 10.1038/s41558-018-0344-1

Riebesell, U., Bach, L. T., Bellerby, R. G. J., Monsalve, J. B., Boxhammer, T., Czerny, J., et al. (2016). Competitive fitness of a predominant pelagic calcifier impaired by ocean acidification. *Nat. Geosci.* 10, 19–23. doi: 10.1038/ngeo2854

Riebesell, U., Czerny, J., von Bröckel, K., Boxhammer, T., Büdenbender, J., Deckelnick, M., et al. (2013). Technical note: a mobile sea-going mesocosm system–new opportunities for ocean change research. *Biogeosciences* 10, 1835–1847. doi: 10.5194/bg-10-1835-2013

Ritchie, R. J. (2006). Consistent sets of spectrophotometric chlorophyll equations for acetone, methanol and ethanol solvents. *Photosynth. Res.* 89, 27–41. doi: 10.1007/s11120-006-9065-9

Rost, B., Richter, K.-U., Riebesell, U. L. F., and Hansen, P. J. (2006). Inorganic carbon acquisition in red tide dinoflagellates. *Plant Cell Environ.* 29, 810–822. doi: 10.1111/j.1365-3040.2005.01450.x

Schulz, K. G., Bellerby, R. G. J., Brussaard, C. P. D., Büdenbender, J., Czerny, J., Engel, A., et al. (2013). Temporal biomass dynamics of an Arctic plankton bloom in response to increasing levels of atmospheric carbon dioxide. *Biogeosciences* 10, 161–180. doi: 10.5194/bg-10-161-2013

Seifert, M., Rost, B., Trimborn, S., and Hauck, J. (2020). Meta-analysis of multiple driver effects on marine phytoplankton highlights modulating role of pCO$_2$. *Glob. Chang. Biol.* 26, 6787–6804. doi: 10.1111/gcb.15341

Sommer, U., Paul, C., and Moustaka-Gouni, M. (2015). Warming and ocean acidification effects on phytoplankton—from species shifts to size shifts within species in a mesocosm experiment. *PLoS One* 10:e0125239. doi: 10.1371/journal.pone.0125239

Spilling, K., Olli, K., Lehtoranta, J., Kremp, A., Tedesco, L., Tamelander, T., et al. (2018). Shifting diatom—dinoflagellate dominance during spring bloom in the Baltic Sea and its potential effects on biogeochemical cycling. *Front. Mar. Sci.* 5:327. doi: 10.3389/fmars.2018.00327

Spilling, K., Schulz, K. G., Paul, A. J., Boxhammer, T., Achterberg, E. P., Hornick, T., et al. (2016). Effects of ocean acidification on pelagic carbon fluxes in a mesocosm experiment. *Biogeosciences* 13, 6081–6093. doi: 10.5194/bg-13-6081-2016

Spivak, A. C., Vanni, M. J., and Mette, E. M. (2011). Moving on up: can results from simple aquatic mesocosm experiments be applied across broad spatial scales? *Freshw. Biol.* 56, 279–291. doi: 10.1111/j.1365-2427.2010.02495.x

Taucher, J., Boxhammer, T., Bach, L. T., Paul, A. J., Schartau, M., Stange, P., et al. (2020). Changing carbon-to-nitrogen ratios of organic-matter export under ocean acidification. *Nat. Clim. Chang.* 11, 52–57. doi: 10.1038/s41558-020-00915-5

Van de Waal, D. B., Brandenburg, K. M., Keuskamp, J., Trimborn, S., Rokitta, S., Kranz, S. A., et al. (2019). Highest plasticity of carbon-concentrating mechanisms in earliest evolved phytoplankton. *Limnol. Oceanogr. Lett.* 4, 37–43. doi: 10.1002/lol2.10102

Vincent, F., and Bowler, C. (2020). Diatoms are selective segregators in global ocean planktonic communities. *mSystems* 5:e00444-19. doi: 10.1128/mSystems.00444-19

Wada, S., Agostini, S., Harvey, B. P., Omori, Y., and Hall-Spencer, J. M. (2021). Ocean acidification increases phytobenthic carbon fixation and export in a warm-temperate system. *Estuar. Coast. Shelf Sci.* 250:107113. doi: 10.1016/j.ecss.2020.107113

Wohlrab, S., John, U., Klemm, K., Eberlein, T., Forsberg Grivogiannis, A. M., Krock, B., et al. (2020). Ocean acidification increases domoic acid contents during a spring to summer succession of coastal phytoplankton. *Harmful Algae* 92:101697. doi: 10.1016/j.hal.2019.101697

Zhang, R., Xia, X., Lau, S. C. K., Motegi, C., Weinbauer, M. G., and Jiao, N. (2013). Response of bacterioplankton community structure to an artificial gradient of pCO$_2$ in the Arctic Ocean. *Biogeosciences* 10, 3679–3689. doi: 10.5194/bg-10-3679-2013